

Exploration of spatio-temporal distribution of aerosol and cloud properties over the Aral Sea Region using MODIS satellite data

Seminar on Cloud-Aerosol Interaction

Faculty of Geography, University of Marburg

Sarah Brüning

Darius A. Görgen

Lecturer

Dr. Boris Thies

Date

December 19, 2019

Number of words

4930

Contents

Contents	i
List of Figures	ii
1 Introduction	1
2 Data and Methods	2
2.1 Study area	2
2.2 Satellite products	3
2.2.1 Aerosol properties	4
2.2.2 Cloud properties	4
2.2.3 Precipitation	5
2.2.4 Relative Humidity	5
2.3 Methodology	6
3 Results	7
3.1 Temporal and spatial variations	7
3.2 Relationship between aerosol and cloud properties	16
4 Discussion	20
5 Conclusion	21
6 References	22
7 Appendix	26

List of Figures

1	Overview of the study domain within the ASB (Grey-scale values represent elevation, solid red lines national boundaries and dashed isolines average yearly sums of precipitation based on CHIRPS for the years 2003-2018).	3
2	Boxplots for yearly sum of precipitation [mm].	8
3	Boxplots for monthly sums of precipitation [mm].	9
4	Spatial distribution of seasonal means for AE for spring (a), summer (b), autumn (c), and winter (d).	12
5	Spatial distribution of seasonal means for SSA for spring (a), summer (b), autumn (c), and winter (d).	13
6	Spatial distribution of seasonal means for COT for spring (a), summer (b), autumn (c), and winter (d).	14
7	Spatial distribution of seasonal means for CER [in microns] for spring (a), summer (b), autumn (c), and winter (d).	14
8	Spatial distribution of seasonal means for CWP [in g/m ²] for spring (a), summer (b), autumn (c), and winter (d).	15
9	Spatial distribution of correlation coefficient rho between AOD and AE during spring (a), summer (b), autumn (c), and winter (d).	17
10	Spatial distribution of correlation coefficient rho between AOD and SSA during spring (a), summer (b), autumn (c), and winter (d).	17
11	Spatial distribution of correlation coefficient rho between AOD and COT during spring (a), summer (b), autumn (c), and winter (d).	18
12	Spatial distribution of correlation coefficient rho between AOD and CER during spring (a), summer (b), autumn (c), and winter (d).	19
13	Spatial distribution of correlation coefficient rho between AOD and CWP during spring (a), summer (b), autumn (c), and winter (d).	19
14	Spatial distribution of linear trend for AOD during spring (a), summer (b), autumn (c), and winter (d).	26
15	Spatial distribution of linear trend for AE during spring (a), summer (b), autumn (c), and winter (d).	26
16	Spatial distribution of linear trend for SSA during spring (a), summer (b), autumn (c), and winter (d).	27

17	Spatial distribution of linear trend for COT during spring (a), summer (b), autumn (c), and winter (d)	27
18	Spatial distribution of linear trend for CER [in microns] during spring (a), summer (b), autumn (c), and winter (d)	28
19	Spatial distribution of linear trend for CWP [in g/m ²] during spring (a), summer (b), autumn (c), and winter (d)	28

1 Introduction

In the last years, an increasing scientific interest has been awoken in terms of the interaction between aerosols and the elements of the hydrological cycle (Ng et al., 2017, p. 1). Precipitation patterns and their influence on human's living environment can be connected with a variety of ecological, economic and social challenges on different spatial extents (Boucher et al., 2013, p. 573 ff.). Especially in semi-arid and arid regions changes in rainfall rates can affect health of local residents (Issanova et al., 2015, p. 3213ff.). Where water is an already scarce resource, further decreases will promote rising vulnerability to external threats (*ibid.*). Regarding this, the Aral Sea region can be seen as a first-class example for investigations between aerosols and rainfall activities (Shen et al., 2019, p. 1). With the desertification of the Aral Sea it has been subject to substantial changes in terms of water availability (Groll et al., 2019, p. 1). Deserts contain a high proportion of mineral aerosols, which may initiate climatological mechanisms of high complexity and, ultimately, a shift in precipitation rates (Boucher et al., 2013, p. 573 ff.). Still, it is hard to quantify the effects on other environmental parameters (Ng et al., 2017, p. 1). The relationship between aerosols and cloud microphysics as well as precipitation patterns remains one of the biggest uncertainties in climate studies (Altaratz et al., 2013, p. 1). Aerosols play a major role in changes of the earth's energy budget (Ng et al., 2017, p. 1) and can be seen as an important component of global climate (Carrico et al., 2003, p. 1). There exist four major terrestrial sources for atmospheric aerosols which, based on their chemical composition, either absorb or scatter incoming solar and terrestrial radiation (Sharif et al., 2015, p. 657f). These direct effects may cool the surface and affect evaporation (Ng et al., 2017, p. 1). Also, aerosols act as cloud condensation nuclei (CCN) leading to more and smaller droplets, which is called the first indirect aerosol effect (Costantino and Bréon, 2010, p. 1). The result is a suppression of precipitation, while the second indirect effect prolongs the cloud's lifetime through the prevention of coalescence favouring the occurrence of extreme events (Ng et al., 2017, p. 2). By heating the cloud, the coverage area is reduced, again leading to a higher amount of radiation on the ground. This attenuates surface evaporation and further decreases rainfall (*ibid.*). A number of studies showed the presence of a strong seasonality in regard to aerosol concentration in Central Asia (Ge et al., 2016, p. 62ff.; Li and Sokolik, 2018, p. 2ff.). The highest values occur in spring while the lowest concentrations have been measured in winter (*ibid.*). However, some studies suggest the indicated perturbation of the hydrological cycle to be more distinct in some places than in others (Ng et al., 2017, p. 2). The goal of this study is to analyse temporal and spatial variations of aerosols in the Aral Sea region in relation to precipitation patterns. Following a prior seminar work regarding the analysis of aerosol and cloud microphysical properties, it continues striving for an adequate estimation of the relationship between hydro-climatological parameters. Therefore, the analysis consists of the investigation of potential trends,

their strength and direction in regard to aerosol concentration to rainfall rates. In order to display the overall effects, cloud microphysical parameters will be included as well as the atmosphere's relative humidity because of its critical role on rainfall variability (Altaratz et al., 2013, p. 1f.; Carrico et al., 2003, p. 2). Some studies suggest high rain rates to be associated with a rising aerosol concentration (Boucher et al., 2013, p. 4). Otherwise, contrary results have been observed as well (Ng et al., 2017, p. 1ff.). In general, time and space seem to be crucial (Grandey et al., 2014, p. 5678ff.). The hygroscopicity of aerosols cause the relative humidity to be one of the most important drivers for the observed relationship between AOD and rainfall (Ng et al., 2017, p. 2f.). When it reaches a certain concentration, it can alter the results of correlation analyses mainly through two effects (Altaratz et al., 2013, p. 1f.). First, relative humidity may cause, dependend on the aerosols' chemical properties, substantial growth of the particles in an humid environment (Carrico et al., 2003, p. 1), leading to coalescence of the droplets (Ng et al., 2017, p. 2ff.). This depicts a rather positive relation between the variables (Grandey et al., 2014, p. 5678). Second, wet scavenging of aerosols through rainfall can occur in a mostly convective environment (Grandey et al., 2014, p. 5680ff.). It acts as an aerosol sink and results in a negative relationship between the aerosol concentration and precipitation or rather relative humidity (*ibid.*). Consequently, a negative correlation may not only reflect suppressed precipitation (Ng et al., 2017, p. 9). Both effects demonstrate the importance of the atmospheres' humidity in questions of aerosol-precipitation relationships and thus will be evaluated in the following study.

2 Data and Methods

2.1 Study area

The Aral Sea basin is located in the border region between Kazakhstan and Uzbekistan (57 – 67 °E, 42 – 49 °N) and acts as the tail-end lake of the contributing rivers Amu Darya and Syr Darya (Figure 1). The study area is part of the global dust belt and shows typical features of a temperate continental climate with semi-arid to arid conditions. The summers are short and hot with a mean of 28.2 °C while winters are long and cold with a mean of -3.6 °C. Precipitation rates are quite low with a mean of about 82.1 *mm/year* and a maximum during winter (Gaynullaev et al., 2012, p. 287). Strong winds are often to be recorded in the study area (Issanova et al., 2015, p. 3213f.). The Aral Sea once has been the fourth largest lake on earth covering a water volume of 1.093 *km*³ in 1960 (Gaynullaev et al., 2012, p. 286). Since then, it has been gradually shrinking due to overexploitation of its natural resources by water abstraction for irrigation agriculture as well as the impacts of climate change (Ge et al., 2016, p. 2; Shen et al., 2019, p. 2031). In the year 2003,

it finally split into eastern and western parts. The exposed lake bed consists of salt soils and loose sand dunes turning the former southern and western part of the lake into the Aralkum desert (Shen et al., 2019, p. 2031f., 2016, p. 624) which comprises of 57.500 km^2 (Opp et al., 2019, p. 3). The landscape is characterized by frequent salt and sand dust storms which may bear several threats to the ecosystem and local human's health (Ge et al., 2016, p. 4). It has been stated that the spatial and temporal dust deposition variability is highly significant (Opp et al., 2019, p. 1ff.).

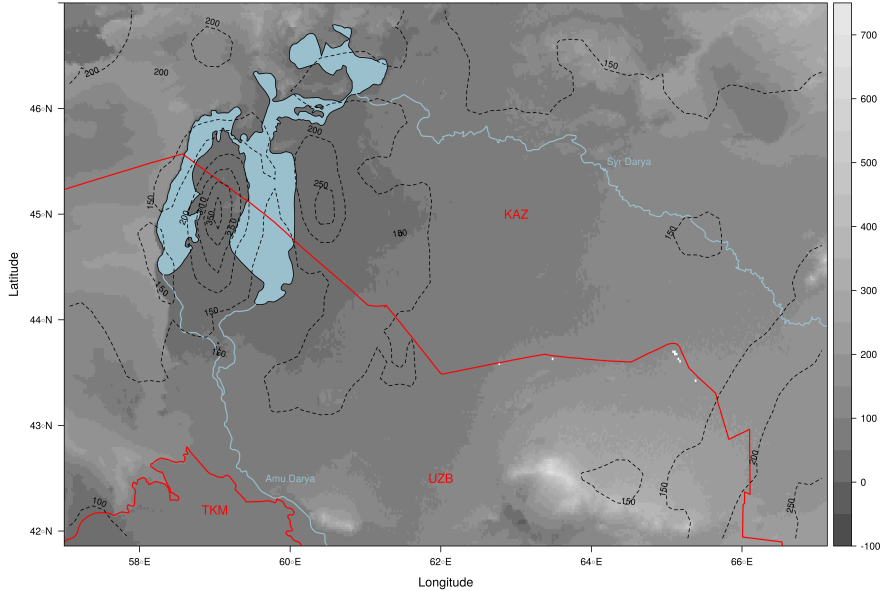


Figure 1: Overview of the study domain within the ASB (Grey-scale values represent elevation, solid red lines national boundaries and dashed isolines average yearly sums of precipitation based on CHIRPS for the years 2003-2018).

2.2 Satellite products

MODIS (Moderate Resolution Imaging Spectroradiometer) data currently is collected by two platforms (TERRA and AQUA) orbiting the Earth on a Sun-synchronous polar orbit. It measures solar and thermal radiation in 36 bands in resolutions ranging from 250 m to 1 km . For this study, daily resolution Level-2 data were used for aerosol (MOD/MYD04) (Levy et al., 2017) and cloud (MOD/MYD06) (Platnick et al., 2017) parameters as well as the corresponding geolocation files (MOD/MYD03) (*MODIS Geolocation Fields 5-Min L1A Swath 1km V006*, 2012).

2.2.1 Aerosol properties

The aerosol optical depth (AOD) were retrieved from the MOD/MYD04 data product based on the Deep Blue algorithm (DB) described by Hsu et al. (2004) and Hsu et al. (2006). DB uses wavelengths in the blue spectrum to overcome the phenomenon of absorbing aerosols darkening the reflectance measured at the sensor over bright surfaces making it more suitable for aerosol retrievals over bright surfaces such as deserts (Hsu et al., 2004). It is applied to clear-sky snow-free pixels over land only and uses the 412, 470/490, 650, 860, 1240 and 2110 μm spectral bands on a final pixel size of 10 x 10 km (Hsu et al., 2013).

Aerosol Optical Depth (AOD): The calculation of AOD is based on a established lookup table which differentiates for several regions around the globe based on dominant aerosol modes found by empirical measurements (Hsu et al., 2004). Two different retrieval techniques can be applied: For moderate dust loadings with $AOD < 0.7$ the algorithm uses a two-channel technique to retrieve aerosol parameters based at 412 and 470/490 μm . Under heavy dust loadings with $AOD > 0.7$ a three-channel technique with the additional 670 μm band may retrieve values for the combination 412 vs. 670 μm and 470/490 vs. 670 μm .

2.2.2 Cloud properties

The algorithm to retrieve cloud optical and microphysical parameters at a nominal resolution of 1 km makes use of the 645, 1640, 2130 and 3750 μm channels over land during daytime. It is applied to cloud overcast pixels only and differentiates the calculation according to the dominant phase of the cloud (Baum et al., 2012). Additionally, information of the surface albedo is included in the algorithm since cloud reflectance is altered due to the underlying surface characteristics. Here, only the parameters describing the cloud's microphysics (COT, CER and CWP) are extracted.

Cloud Effective Radius (CER) and Cloud Optical Thickness (COT): CER and COT are derived from water-absorbing bands of MODIS (1.6, 2.1, 3.7 μm) coupled with non-absorbing bands (0.65, 0.86 and 1.2 μm) (Platnick et al., 2003). The algorithm uses a radiative transfer model to calculate a reflected intensity field for combinations of CER and COT. Both parameters are then retrieved based on the measured reflectance. With the introduction of the algorithm version C6 the retrieval of cloud parameters for optical thin clouds has been enabled (Platnick et al., 2017). For this study the data layers which retrieve CER and COT based on the relation between 2.1 μm and 0.65, 0.86 and 1.2 μm were used.

Cloud Water Path (CWP): The CWP is directly linked to CER and COT and refers to the total liquid water amount found in the atmospheric column above a given pixel. It can be calculated in a simplified manner by

use of Formula 2:

$$CWP = y * CER * COT \quad (1)$$

This form of the calculation is beneficial for satellite-based measurements, since CWP can be estimated with information on COT and CER only. The term y is either determined by adiabatic assumptions (Wood, 2006) or the assumption of a vertically homogeneous water column (Stephens et al., 1978) becoming either the ratio $5/9$ or $2/3$, respectively.

2.2.3 Precipitation

Precipitation (P): Monthly sums of precipitation are derived from the CHIRPS dataset. This dataset is established by taking long-term monthly average data from ground stations in conjunction with observations from five satellite missions to establish a local regression model with a moving window for each grid cell of 0.05° in size (Funk et al., 2015, p. 3f.). The independent variables in the local regressions consist always of the longitude and latitude information as well as one to three additional variables representing either the local elevation, the slope or satellite observations. Potential residuals in comparison to the FAO climate normals are interpolated using inverse distance weighting and are then added to the local estimates (Funk et al., 2015, p. 3). In a last step, for every pixel the five nearest ground stations are used to apply another inverse distance weighting algorithm. Here, an estimate of the decorrelation slope from the predicted precipitation and the observed precipitation at the neighbouring stations are used to calculate a weighted average (Funk et al., 2015, p. 3).

2.2.4 Relative Humidity

Relative Humidity (RH): RH is retrieved using the ERA-5 reanalysis dataset processed by the European Centre for Medium-Range Weather Forecasts (ECMWF) (Forecasts, 2017). This dataset combines observations and model predictions to get a comprehensive model of global atmospheric conditions at small time steps and a nominal resolution of 31km at the ground, however the data has been regridded to 0.25° . The atmosphere is modeled in 137 vertical levels from the surface to 1 Pa. Here, we used the monthly aggregates of RH only for the first seven atmospheric layers (1000 hPa - 850 hPa) since the other datasets were also summarized to monthly aggregates. 850 Pa was considered an appropriate height level, since local aerosol transports in the region are merely reported to be found above 5 km in height (Chen et al., 2013).

2.3 Methodology

AOD and the cloud parameters were extracted from the respective MODIS datasets using the HEG-Tool (HDF-EOS To GeoTIFF Conversion Tool). It enables a selection of the cloud and aerosol properties clipping the data directly to the area of interest which is leaned on the shape of the study area used by (Ge et al., 2016). The cloud parameters (at 6km nominal resoultion) were resampled to the 10km nominal resoultion of the AOD dataset. The observations of single MODIS overflights were then aggregated to a monthly temporal-resolution, and means were calculated for four different seasons (Spring: March, April, May; Summer: June, July, August; Autumn: September, October, November; Winter: December, January, February) for every year between 2003 to 2018.

The CHIRPS dataset already represents monthly aggregates. The cell values were resampled to the 10km resoultion of the MODIS data and seasonal aggregates were calculated as described above. For RH, the process was basically identical, except that the median was calculated across the seven vrtival layers, before the data was resampled to the same resoultion as the other datasets.

To retrieve the correlation between AOD and P and to generate insights to the underlying processes we conduct a number of correlation analysis between these two parameters, while eleminating the influence of cloud parameteres and RH. For this approach, we firstly cheked if the data fullfills the assumptions to calcualte Pearsons correlation. All variables are continous in form. Pearsons correlation additionally is sensitive for outliers. Similiarly to other studys we thus excluded exceptional high AOD values above 0.3. Also, we assume linear relationships between the variables for values below the AOD threshold of 0.3. We then calculated the correlation coefficient betwenn AOD and P while controlling for any other variable. This is achieved by calculating the partial correlation. Partial correlation is used as a measure of the linear dependence between two variables while controlling for the influences of a third. In fact, not the original values of AOD and P are fitted, but rather the residuals which were calculated by using the control variable as a predictor. Thus, only the proportion of variance which cannot be explained by the control variable is subject to the correlation analysis (Salkind, 2010). This approach has been chosen by a number of recent studies investigating relationships between aerosols and cloud microphysics as well as precipitations and seems reasonable to achive both, investigating the “true” realtionship between AOD and P in a complex field of intervening processes and effects and to deliver indications for the dominant processes driving this relationship (Engström and Ekman, 2010; Gryspeerdt et al., 2014; Ng et al., 2017).

The results of this analysis are presented on a pixel basis for each season to display spatial and temporal differences. Additionally, the correlation of all pixels which show a significant relationship at the 95%

confidence interval is calculated to investigate the overall direction and strength of correlation between aerosol and cloud parameters (Alam et al., 2010, p. 1170f.).

3 Results

3.1 Temporal and spatial variations

The temporal and spatial variations of several aerosol and cloud parameters have been presented in the previous seminar paper. Here, we only represent the additional parameters P and RH.

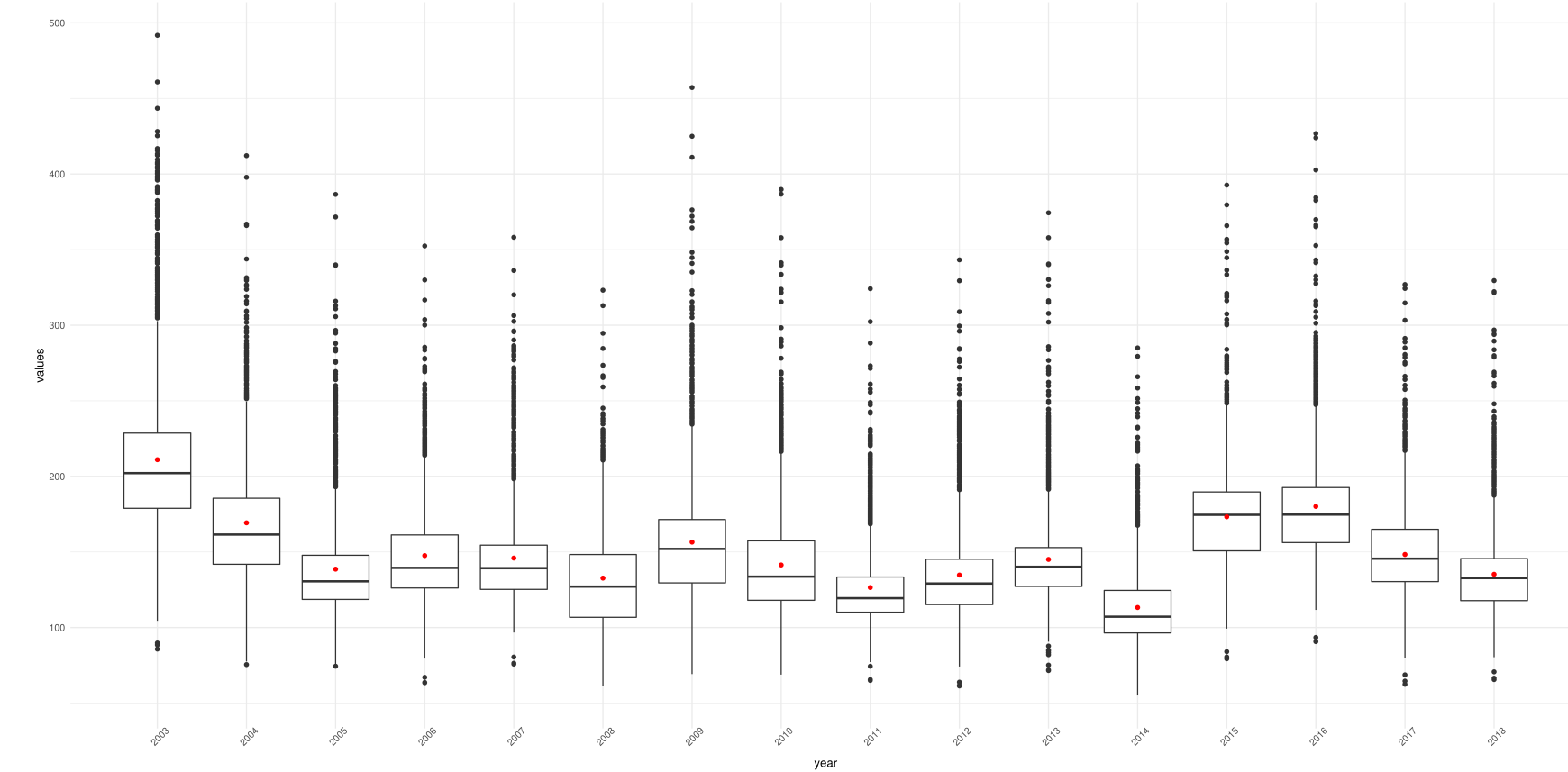


Figure 2: Boxplots for yearly sum of precipitation [mm].

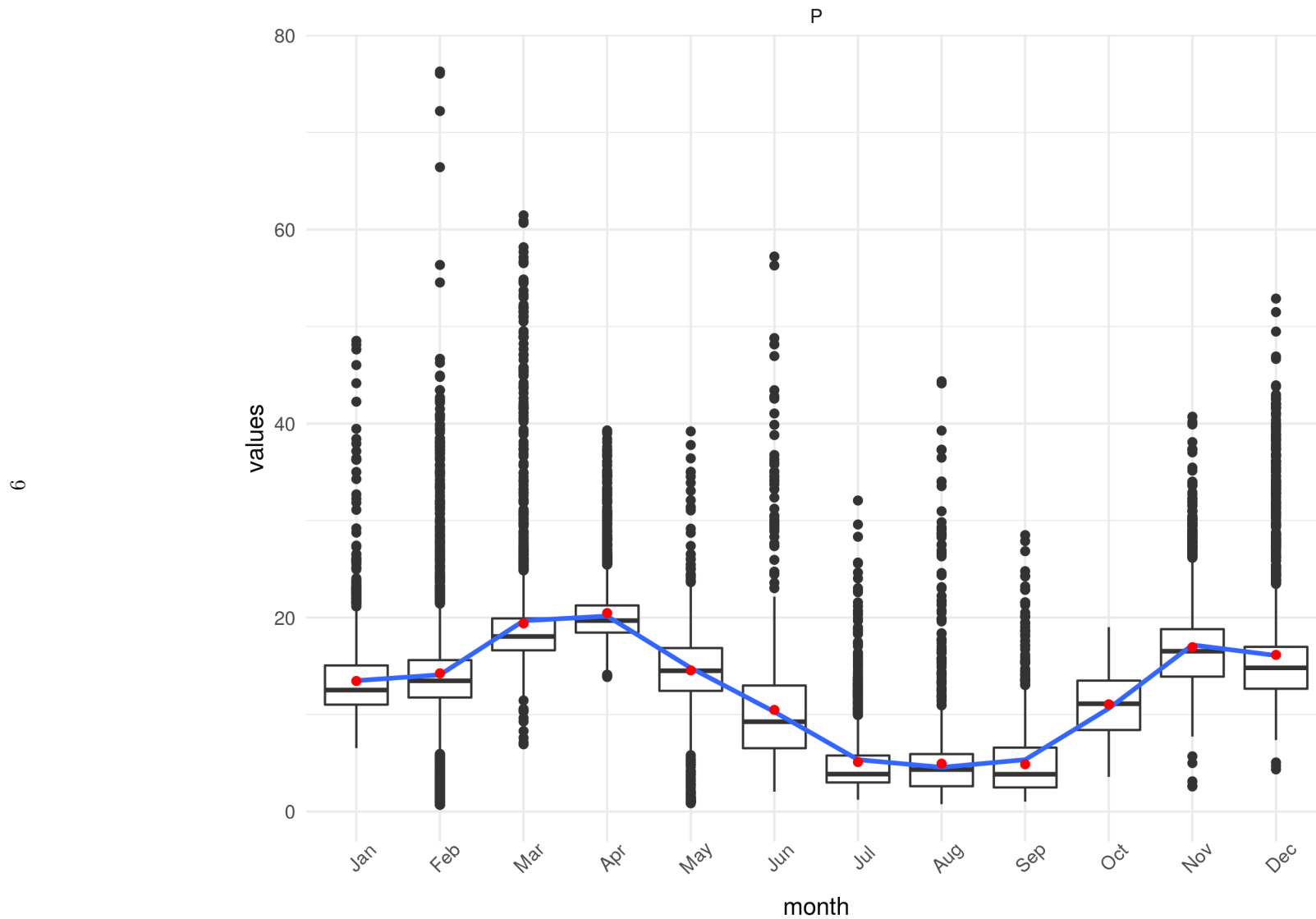
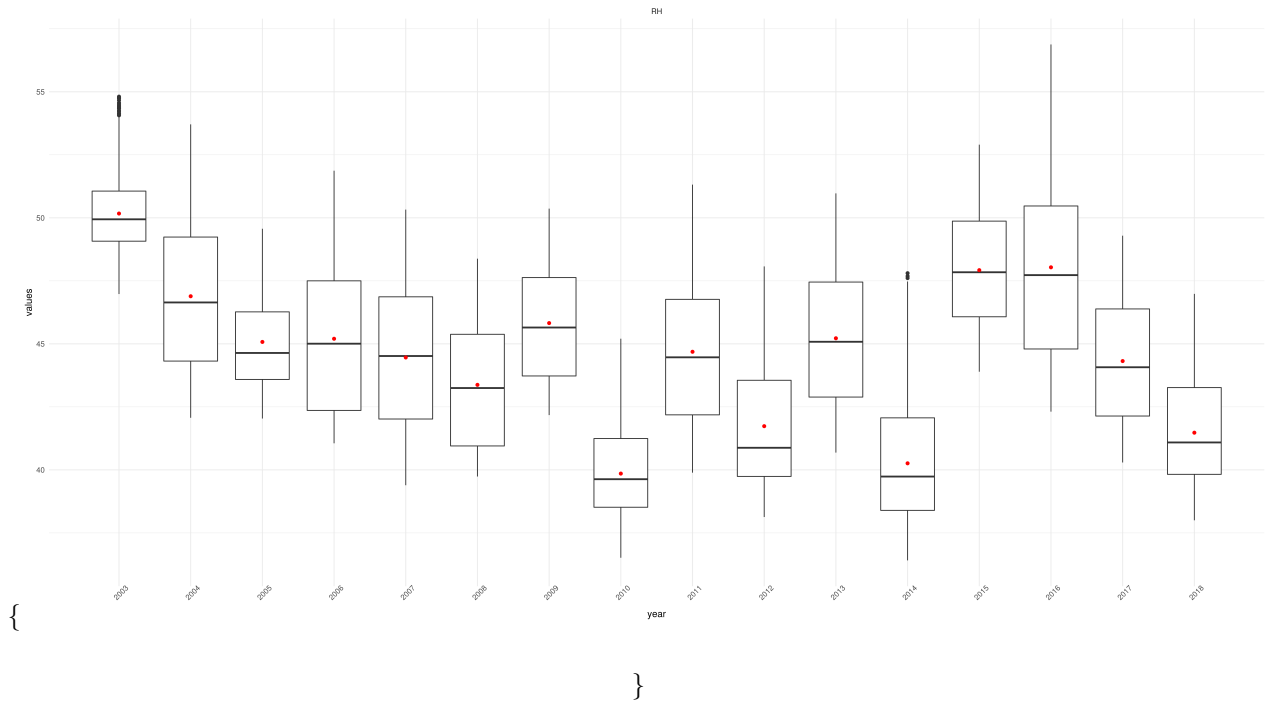


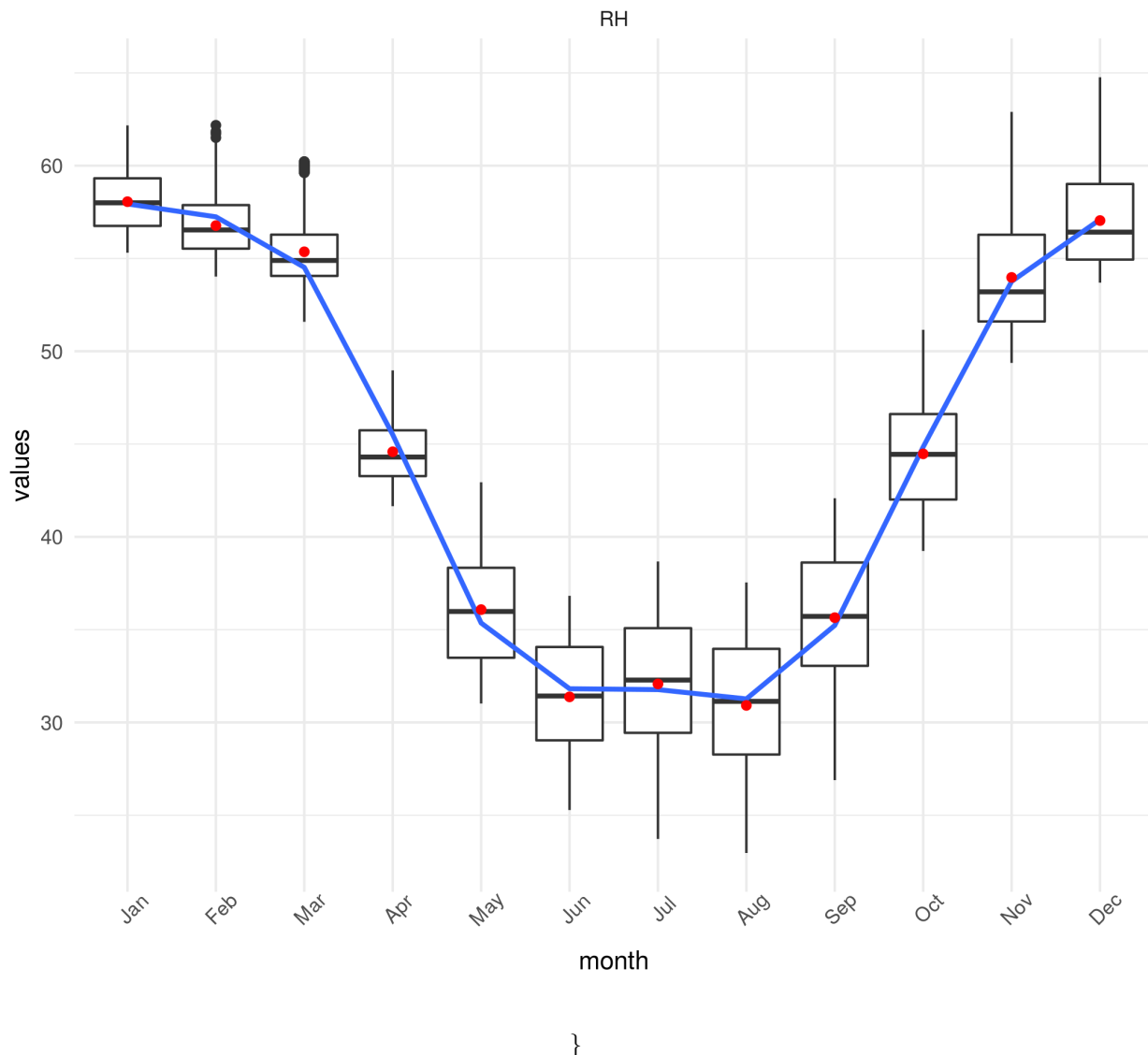
Figure 3: Boxplots for monthly sums of precipitation [mm].

\begin{landscape} \begin{figure}



\caption{Boxplots for yearly median of relative humidity [%].} \end{figure}

\begin{figure}



\caption{Boxplots for monthly median relative humidity [%].} \end{figure} \end{landscape}

Aerosol properties trend detection: The AOD is higher around and North-West of the Aral Sea with maximum values in spring and autumn (Figure 6). The long-term trend analysis shows an increasing trend close to the Aral Sea and Aralkum, while the values further away tend to decrease (Appendix, Figure 17).

The slopes picture a rather small change for the mean values.

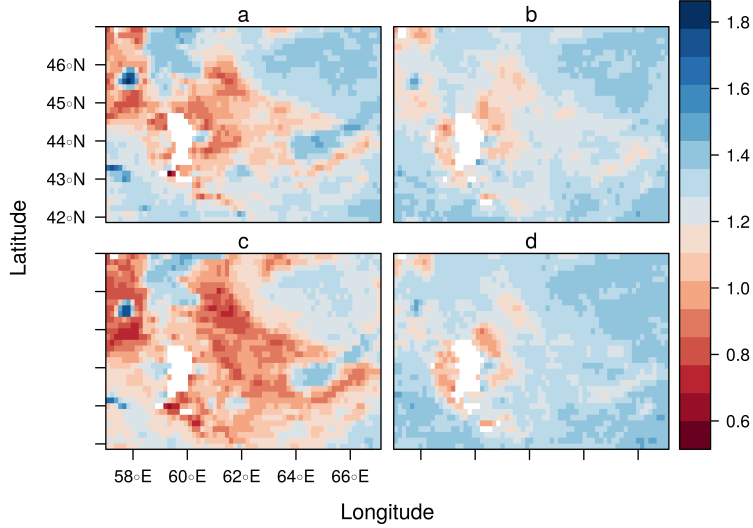


Figure 4: Spatial distribution of seasonal means for AE for spring (a), summer (b), autumn (c), and winter (d).

Contrary to this, the AE reaches its lowest values in spring and autumn, while the maximum appears in summer and winter (Figure 7). Overall, the AE increases with rising distance to Aral Sea. In spring and autumn, a great proportion of the areas East and West to the Aralkum show values of $\text{AE} < 1.0$. The trend detection depicts in spring, summer and winter mostly increasing values (Appendix, Figure 18). Only individual pixels show a significant increase especially in the East of the Aral Sea. In autumn, decreasing trends are dominating, but still can only be applied to the areas close to the lake surface and the Aralkum.

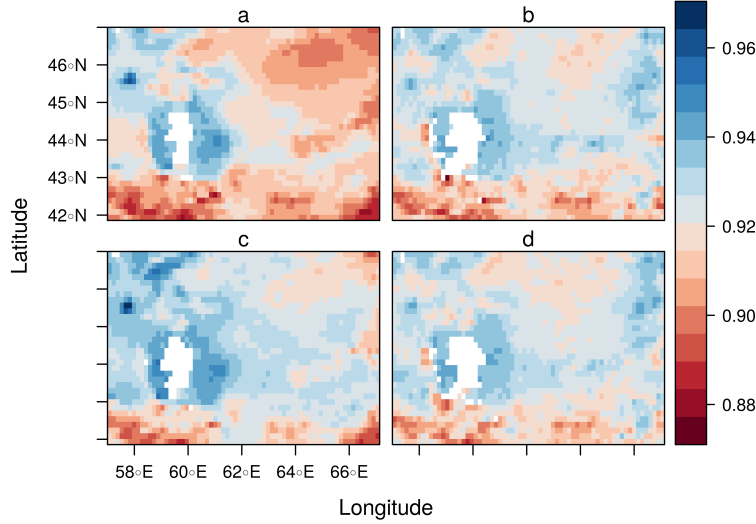


Figure 5: Spatial distribution of seasonal means for SSA for spring (a), summer (b), autumn (c), and winter (d).

The SSA shows a considerable spatial pattern with higher values around the Aral Sea (Figure 8). In the South and North-East of the study area, values are considerably lower. Especially in spring, there is a high variation between the individual regions. As for the trend detection, mostly decreasing trends are observed except for the spring season (Appendix, Figure 19). Close to the surface of the Aral Sea and the Aralkum, however, stronger increases in SSA are found during spring and autumn and fewer steep decreases in summer and winter. In contrast to the other aerosol properties, most of the pixels are characterized by a significant detection of a linear decreasing long-term trend. In contrast, a monotonous trend detection for AOD and AE is not possible on a whole scale level. Here, significant trends only appear for individual pixels with a high spatial and temporal divergence. In addition, all slopes only display slight changes as the slopes are weakly defined.

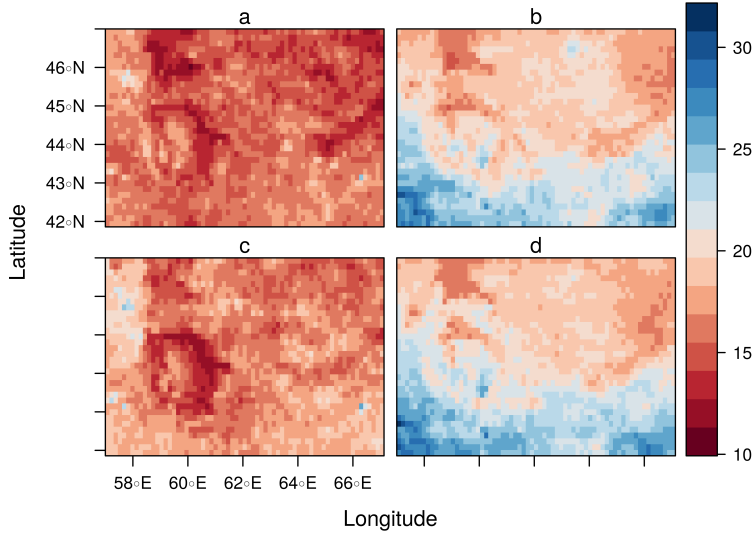


Figure 6: Spatial distribution of seasonal means for COT for spring (a), summer (b), autumn (c), and winter (d).

Cloud properties trend detection: The COT depicts a seasonal cycle with lowest values in spring and autumn and higher values in summer and winter (Figure 9). During the latter ones, maximum values are reached in the southern region. The Aral Sea and the Aralkum are visible as regions with moderately lower values. The trend analysis shows the dominance of positive slopes in spring and autumn especially around the Aral Sea and Aralkum whereas values in the other seasons are rather decreasing (Appendix, Figure 20).

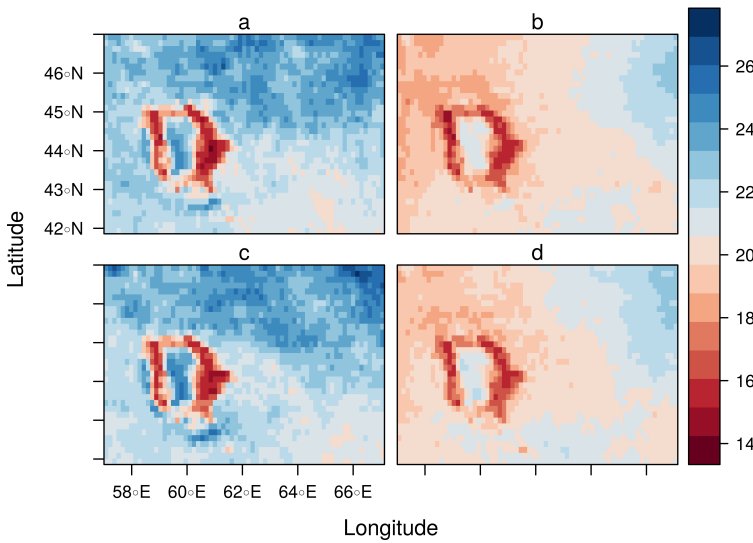


Figure 7: Spatial distribution of seasonal means for CER [in microns] for spring (a), summer (b), autumn (c), and winter (d).

Also, these regions are shown as well as a clear shape in all seasons for CER (Figure 10). They are characterized by very low values in contrast to the rest of the study area. Apart from that, values are generally higher in spring and autumn with the spatial maximum appearing in the North-East of the study area, while throughout all seasons lower values can be observed South-East and West of the Aral Sea's surface. The trend analysis agrees with the pattern of a decreasing CER during spring, autumn and winter especially around the lake and the Aralkum (Appendix, Figure 21).

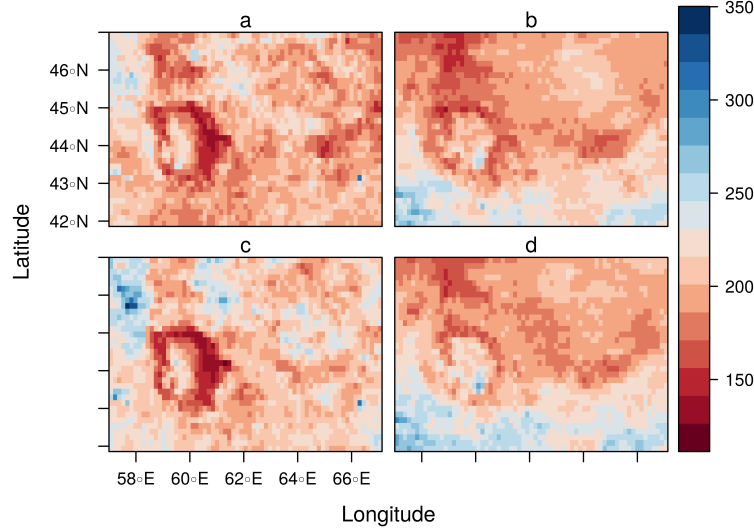


Figure 8: Spatial distribution of seasonal means for CWP [in g/m²] for spring (a), summer (b), autumn (c), and winter (d).

Minimal values for CWP during all seasons are observed around the Aral Sea as well while they increase only in the South of the study area during summer and winter (Figure 11). No clear seasonal differences are observed, instead, a diverging seasonal pattern dominates (Appendix, Figure 22). During spring and autumn, there is a very diverse pattern of trends. The slopes are positive during summer and winter in close distance to the lake and the Aralkum. These pixels are the only ones showing a significant trend during these seasons, but the rest of the study area is otherwise characterized by a decreasing CWP. Like for the aerosol properties, a linear trend detection for all cloud properties on a whole scale level is not possible. Individual parameters imply the existence of a trend, but most pixels do not apply to the significance level.

3.2 Relationship between aerosol and cloud properties

Relationship between aerosol properties: The analysis of the relationship between AOD and AE shows a seasonal dependence with mainly a moderate to high negative correlation (Table 1). The spatial analysis implies mostly negative values for the study area with the strongest relationship in the central region. They tend to be generally stronger in spring and autumn.

Close to the Aral Sea, there are some pixels showing a positive correlation, but only negative correlated pixels can be seen as statistically significant (Figure 12). The relationship between the AOD and SSA depicts an opposing and also weaker relationship, with more positive correlations and a higher spatial diversity (Table 1). However, again only negative correlations are found to be statistically significant especially during summer and autumn (Figure 13).

Table 1: Correlation coefficients between aerosol and cloud parameters by season.

parameters	spring	summer	autumn	winter
AE vs. SSA	-0.54	-0.11	-0.24	-0.23
AE vs. AOD	-0.77	-0.64	-0.77	-0.65
SSA vs. AOD	0.52	0.11	0.34	0.22
AOD vs. CER	-0.2	-0.15	-0.2	-0.1
AOD vs. CWP	0	-0.11	-0.08	-0.07
AOD vs. COT	0.08	-0.06	-0.04	-0.05

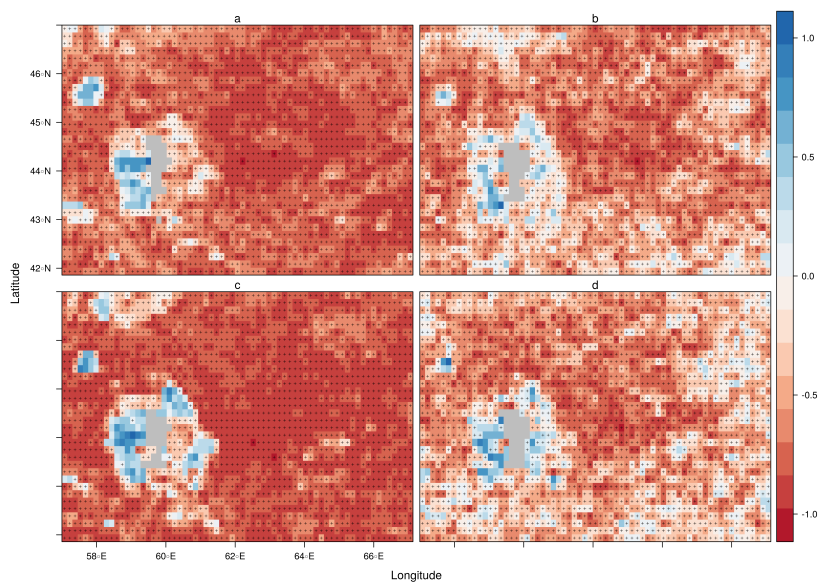


Figure 9: Spatial distribution of correlation coefficient rho between AOD and AE during spring (a), summer (b), autumn (c), and winter (d).

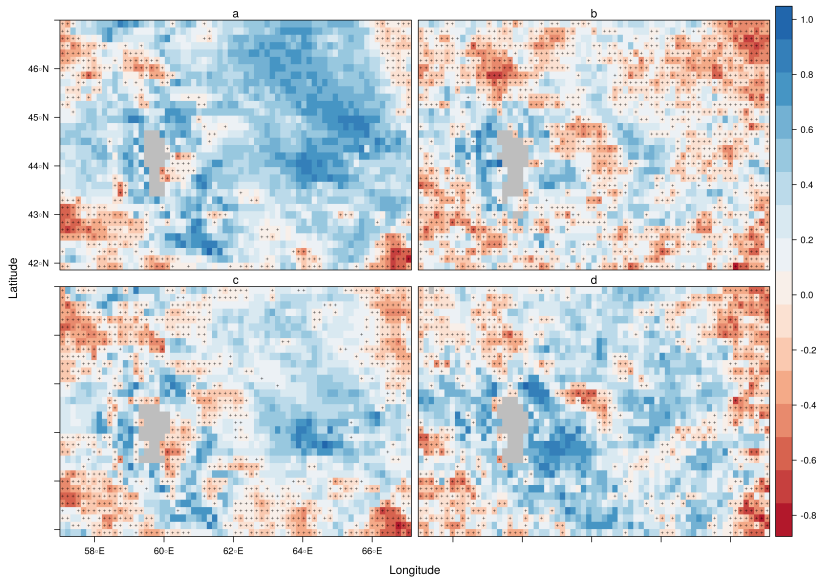


Figure 10: Spatial distribution of correlation coefficient rho between AOD and SSA during spring (a), summer (b), autumn (c), and winter (d).

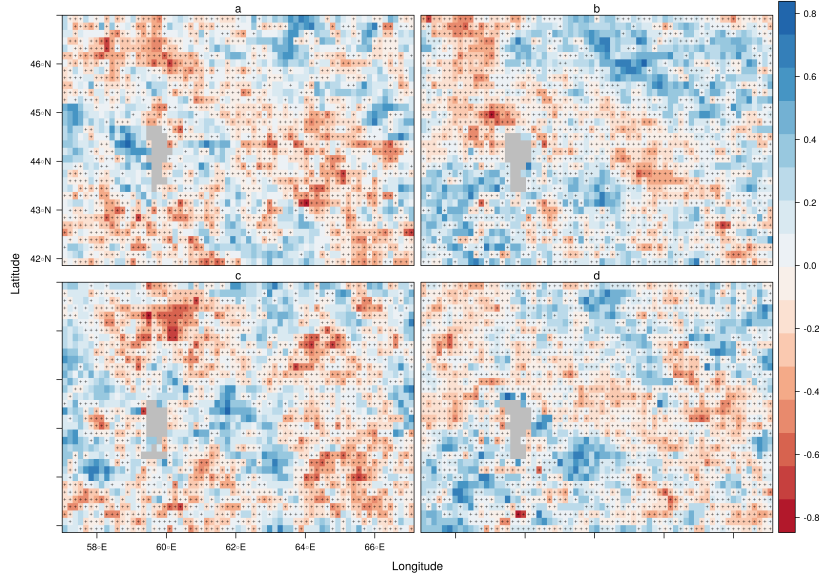


Figure 11: Spatial distribution of correlation coefficient rho between AOD and COT during spring (a), summer (b), autumn (c), and winter (d).

Relationship between AOD and COT: The relationship between AOD and COT shows overall very low to low correlation coefficients (Table 1). Based on this a highly mixed distribution of negative and positive correlation coefficients can be identified. The variation makes it hard to find a clear pattern, though there is a band of significant negative correlations from the North-West to the South-East of the study area. Most pixels showing a negative sign are statistically significant, even though the overall strength of the relationship is questionable (Figure 14).

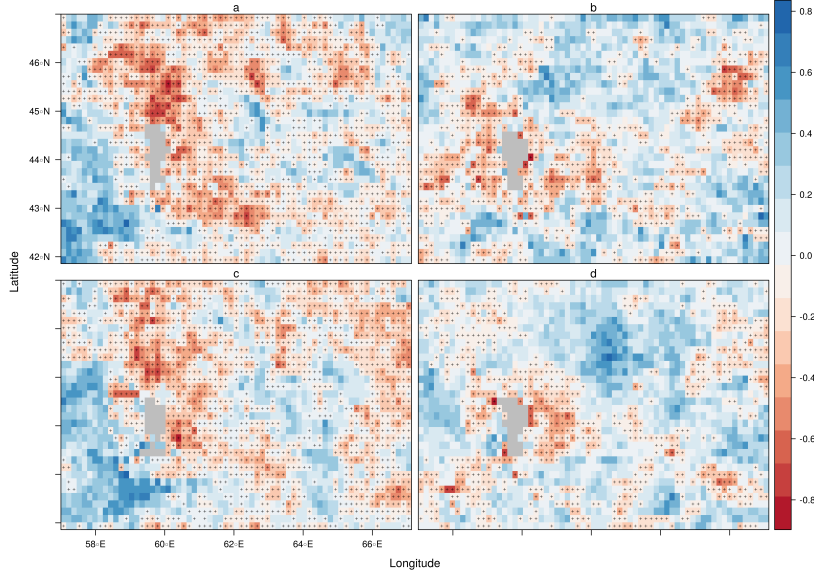


Figure 12: Spatial distribution of correlation coefficient rho between AOD and CER during spring (a), summer (b), autumn (c), and winter (d).

Relationship between AOD and CER: The AOD and the CER have a generally low to medium negative correlation (Table 1). The spatial analysis shows only negative correlations to be statistically significant. They tend to occur mostly in the central region of the study area as well as North and East of the Aral Sea and the Aralkum (Figure 15). The strongest relationship is observed during in spring and autumn (ibid.).

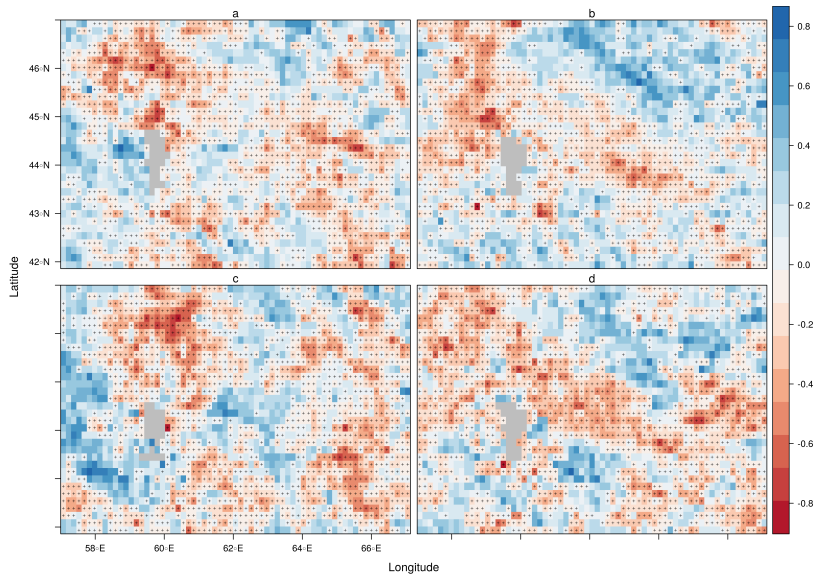


Figure 13: Spatial distribution of correlation coefficient rho between AOD and CWP during spring (a), summer (b), autumn (c), and winter (d).

Relationship between AOD and CWP: The relationship between AOD and the CWP is negative in total, with positive values only in spring. All values indicate a very low to low correlation (Table 1). The correlation maps show spatial highly deviating relationships with the highest values to be found North and West of the Aral Sea (Figure 16). Instead of a seasonal cycle, again a spatial pattern with a band of negative slopes on a highly significant level can be observed. Positive slopes rarely show significance throughout all seasons.

4 Discussion

Most of the depicted parameters do not show a monotonous trend. Contrary to former assumptions, the aerosol concentration does not show a linear increase from 2003 – 2018. While the size distribution reveals deviating values for AE, this proxy cannot be uniformly applied for estimating the aerosol type (Huang et al., 2014, p. 400ff.). Only in spring and autumn and together with an increasing absorption rate through decreasing SSA the hypotheses of dominating mineral dust is supported in some parts of the study area. For the cloud properties, no monotonous trend is visible. It is indicated that COT, CER and CWP are decreasing, but the statistical significance of these results is uncertain. Therefore, an analysis of the clouds microphysics is difficult. Also, the seasonal cycles which were assumed to fit together with the supposed relationships between aerosol and cloud properties do not overlap. Instead, the relationships between the individual parameters display rather weak correlations. In contrast to other studies in similar regions of Central Asia which obtained stronger results, their information value needs to be reconsidered (Alam et al., 2010, p. 1165ff.; Sharif et al., 2015, p. 660ff.).

In addition, the first and second indirect aerosol effect were analysed. Together with a rising AOD, a lower CER and an increasing COT, the Twomey effect may be assumed (Huang et al., 2014, p. 406ff.). The existence of the second indirect effect was investigated inspecting the correlation between AOD and CWP (*ibid.*). For small parts of the region – especially around the Aralkum – these hypotheses seem to be applicable. There are hints for a precipitation feedback loop because of the overall negative correlation between AOD and the cloud properties. But since the data show a tremendous variability in parameter's relationships and overall mostly low correlations, no definite statement for answering the scientific question is possible. The hypotheses set before can be neither confirmed nor denied. The analysis illustrates the complexity and difficulty of aerosol-cloud interactions as most relationships cannot be explained by merely the correlation coefficients used in this study. As pictured before, the aerosol cloud interactions demonstrate a high spatial and temporal variability with generally stronger characteristics in spring and autumn. Since all results cannot be confirmed for the whole study area and every parameter, they need to be treated with

caution.

Instead, the influence of other parameters becomes apparent. These include not only meteorological conditions (Sharif et al., 2015, p. 657), but also the importance of external effects (Huang et al., 2006, p. 4).

Mesoscale convective systems may cover local processes and can disguise the origin of interacting factors (Sharif et al., 2015, p. 660ff.). As no trajectory analysis is included, the origin of the aerosols stays unknown (*ibid.*). Furthermore, changes in the land use, e.g. through irrigation, may lead to more greening and less aerosol deposition, thus modifying the correlation results (Jin et al., 2017, p. 2f.). Also, the vertical structure of the clouds is an important feature in order to analyse the effects of aerosols on their hydrological cycle. Regarding these, the analysis needs to include more precise parameters to ensure reliable results (Costantino and Bréon, 2010, p. 4f.; Li and Sokolik, 2018, p. 22ff.). Apart from that the aggregation of the data can lead

to an over- or underestimation of the estimated effects (Sayer et al., 2013, p. 7864ff.). In addition, the dimension of the existing retrieval bias in the MODIS data caused by the water surface of the Aral Sea stays unknown thus not leading to strictest results (Jin et al., 2017, p. 9f.). Nevertheless, there seems to be potential for optimizing (Li and Sokolik, 2018, p. 22ff.). The combination of instrumental and spatial difficulties inhibits a more detailed statement in regard to answering the scientific questions and hypotheses assumed before. This said, it is necessary to include a variety of possible influences in the analysis as well as taking further investigations in the cloud microphysical properties. Future research needs to take a closer look at the changes in the hydrological cycle: the feedback loop for rainfall rates may be implied, but its dimension and quantification in the region remain unclear.

5 Conclusion

As a result, the quantification of the aerosol-cloud interaction in the Aral Sea region includes several difficulties in gaining a reliable output. An accurate answer for the scientific questions needs to be replaced by a first approximation. The existence of a relationship between most of the aerosol and cloud properties can be assumed, but their strength, direction and possible consequences need to be further investigated. The results of this study may provide an overview for a study area that has not been object of this kind of research before. The problems that occurred can be led back to either instrumental and methodical issues or the complexity of natural processes. As the study itself dealt with a highly relevant topic many uncertainties in dealing with cloud microphysics still exist to this point. It is a future challenge to pursue solutions to these obstacles. Especially in highly vulnerable regions like the Aral Sea, changes in the hydrological pattern originating to aerosol concentration alterations may inhabit considerable threats to humans and nature,

e.g. the expansion of deserts and ongoing salinization. Therefore, an estimation of precipitation patterns and shifts as well as the clouds vertical structure and more precise aerosol type analyses are crucial for future research.

6 References

- Alam, K., Iqbal, M.J., Blaschke, T., Qureshi, S., Khan, G., 2010. Monitoring spatio-temporal variations in aerosols and aerosol-cloud interactions over Pakistan using MODIS data. *Advances in Space Research* 46, 1162–1176. <https://doi.org/10.1016/j.asr.2010.06.025>
- Altaratz, O., Bar-Or, R.Z., Wollner, U., Koren, I., 2013. Relative humidity and its effect on aerosol optical depth in the vicinity of convective clouds. *Environmental Research Letters* 8. <https://doi.org/10.1088/1748-9326/8/3/034025>
- Baum, B.A., Menzel, W.P., Frey, R.A., Tobin, D.C., Holz, R.E., Ackerman, S.A., Heidinger, A.K., Yang, P., 2012. MODIS Cloud-Top Property Refinements for Collection 6. *Journal of Applied Meteorology and Climatology* 51, 1145–1163. <https://doi.org/10.1175/JAMC-D-11-0203.1>
- Boucher, O., Randall, D., Artaxo, P., Bretherton, C., Feingold, G., Forster, P., Kerminen, V.-M., Kondo, Y., Liao, H., Lohmann, U., Rasch, P., Satheesh, S., Sherwood, S., Stevens, B., Zhang, X., 2013. Clouds and Aerosols, in: Stocker, T., Qin, D., Plattner, G.-K., Tignor, M., Allen, S., Boschung, J., Nauels, A., Xia, Y., Bex, V., Midgley, P. (Eds.), *Climate Change 2013: The Physical Science Basis. Contribution of Working Group I to the Fifth Assessment Report of the Intergovernmental Panel on Climate Change*. Cambridge University Press, Cambridge, United Kingdom; New York, NY, USA., pp. 465–657. <https://doi.org/10.1017/CBO9781107415324.015>
- Carrico, C.M., Kus, P., Rood, M.J., Quinn, P.K., Bates, T.S., 2003. Mixtures of pollution, dust, sea salt, and volcanic aerosol during ACE-Asia: Radiative properties as a function of relative humidity. *Journal of Geophysical Research D: Atmospheres* 108. <https://doi.org/10.1029/2003jd003405>
- Chen, B.B., Sverdlik, L.G., Imashev, S.A., Solomon, P.A., Lantz, J., Schauer, J.J., Shafer, M.M., Artamonova, M.S., Carmichael, G.R., 2013. Lidar Measurements of the Vertical Distribution of Aerosol Optical and Physical Properties over Central Asia. *International Journal of Atmospheric Sciences* 2013, 1–17. <https://doi.org/10.1155/2013/261546>
- Costantino, L., Bréon, F.M., 2010. Analysis of aerosol-cloud interaction from multi-sensor satellite

- observations. *Geophysical Research Letters* 37. <https://doi.org/10.1029/2009GL041828>
- Engström, A., Ekman, A.M., 2010. Impact of meteorological factors on the correlation between aerosol optical depth and cloud fraction. *Geophysical Research Letters* 37, 1–4.
<https://doi.org/10.1029/2010GL044361>
- Forecasts, E.C. for M.-R.W., 2017. ERA5 Reanalysis (0.25 Degree Latitude-Longitude Grid).
<https://doi.org/https://doi.org/10.5065/BH6N-5N20>
- Funk, C., Peterson, P., Landsfeld, M., Pedreros, D., Verdin, J., Shukla, S., Husak, G., Rowland, J., Harrison, L., Hoell, A., Michaelsen, J., 2015. The climate hazards infrared precipitation with stations - A new environmental record for monitoring extremes. *Scientific Data* 2, 1–21. <https://doi.org/10.1038/sdata.2015.66>
- Gaynullaev, B., Chen, S.-C., Gaynullaev, D., 2012. Changes in water volume of the Aral Sea after 1960. *Applied Water Science* 2, 285–291. <https://doi.org/10.1007/s13201-012-0048-z>
- Ge, Y., Abduwaili, J., Ma, L., Liu, D., 2016. Temporal Variability and Potential Diffusion Characteristics of Dust Aerosol Originating from the Aral Sea Basin, Central Asia. *Water, Air, and Soil Pollution* 227.
<https://doi.org/10.1007/s11270-016-2758-6>
- Grandey, B.S., Gururaj, A., Stier, P., Wagner, T.M., 2014. Rainfall-aerosol relationships explained by wet scavenging and humidity. *Geophysical Research Letters* 41, 5678–5684.
<https://doi.org/10.1002/2014GL060958>
- Groll, M., Opp, C., Issanova, G., Vereshagina, N., Semenov, O., 2019. Physical and Chemical Characterization of Dust Deposited in the Turan Lowland (Central Asia). *E3S Web of Conferences* 99, 03005.
<https://doi.org/10.1051/e3sconf/20199903005>
- Gryspeerdt, E., Stier, P., Grandey, B.S., 2014. Cloud fraction mediates the aerosol optical depth-cloud top height relationship. *Geophysical Research Letters* 41, 3622–3627. <https://doi.org/10.1002/2014GL059524>
- Hsu, N.C., Jeong, M.J., Bettenhausen, C., Sayer, A.M., Hansell, R., Seftor, C.S., Huang, J., Tsay, S.C., 2013. Enhanced Deep Blue aerosol retrieval algorithm: The second generation. *Journal of Geophysical Research Atmospheres* 118, 9296–9315. <https://doi.org/10.1002/jgrd.50712>
- Hsu, N.C., Tsay, S.C., King, M.D., Herman, J.R., 2006. Deep Blue retrievals of Asian aerosol properties during ACE-Asia. *IEEE Transactions on Geoscience and Remote Sensing* 44, 3180–3195.
<https://doi.org/10.1109/TGRS.2006.879540>
- Hsu, N.C., Tsay, S.C., King, M.D., Herman, J.R., 2004. Aerosol properties over bright-reflecting source

- regions. IEEE Transactions on Geoscience and Remote Sensing 42, 557–569.
<https://doi.org/10.1109/TGRS.2004.824067>
- Huang, J., Lin, B., Minnis, P., Wang, T., Wang, X., Hu, Y., Yi, Y., Ayers, J.K., 2006. Satellite-based assessment of possible dust aerosols semi-direct effect on cloud water path over East Asia. Geophysical Research Letters 33. <https://doi.org/10.1029/2006GL026561>
- Huang, J., Wang, T., Wang, W., Li, Z., Yan, H., 2014. Climate effects of dust aerosols over east asian arid and semiarid regions. <https://doi.org/10.1002/2014JD021796>
- Issanova, G., Abuduwaili, J., Galayeva, O., Semenov, O., Bazarbayeva, T., 2015. Aeolian transportation of sand and dust in the Aral Sea region. International Journal of Environmental Science and Technology 12, 3213–3224. <https://doi.org/10.1007/s13762-015-0753-x>
- Jin, Q., Wei, J., Yang, Z.L., Lin, P., 2017. Irrigation-induced environmental changes around the Aral Sea: An integrated view from multiple satellite observations. <https://doi.org/10.3390/rs9090900>
- Levy, R., Hsu, C., Sayer, A., Mattoo, S., Lee, J., 2017. MODIS Atmosphere L2 Aerosol Product. NASA MODIS Adaptive Processing System, Goddard Space Flight Center.
https://doi.org/10.5067/MODIS/MOD04_L2.061; [10.5067/MODIS/MYD04_L2.061](https://doi.org/10.5067/MODIS/MYD04_L2.061)
- Li, L., Sokolik, I.N., 2018. Analysis of dust aerosol retrievals using satellite data in Central Asia. Atmosphere 9. <https://doi.org/10.3390/atmos9080288>
- MODIS Geolocation Fields 5-Min L1A Swath 1km V006, 2012.. MODIS Characterization Support Team, Level 1; Atmosphere Archive; Distribution System (LAADS). <https://doi.org/10.5067/MODIS/MOD03.006>; [10.5067/MODIS/MYD03.006](https://doi.org/10.5067/MODIS/MYD03.006)
- Ng, D.H.L., Li, R., Raghavan, S.V., Liong, S.Y., 2017. Investigating the relationship between Aerosol Optical Depth and Precipitation over Southeast Asia with Relative Humidity as an influencing factor. Scientific Reports 7, 1–13. <https://doi.org/10.1038/s41598-017-10858-1>
- Opp, C., Groll, M., Semenov, O., Vereshagina, N., Khamzina, A., 2019. Impact of the Aral Sea Syndrome - the Aralkum as a Man-Made Dust Source. E3S Web of Conferences 99, 03003.
<https://doi.org/10.1051/e3sconf/20199903003>
- Platnick, S., King, M.D., Ackerman, S.A., Menzel, W.P., Baum, B.A., Riédi, J.C., Frey, R.A., 2003. The MODIS cloud products: Algorithms and examples from terra. IEEE Transactions on Geoscience and Remote Sensing 41, 459–472. <https://doi.org/10.1109/TGRS.2002.808301>

- Platnick, S., Meyer, K.G., King, M.D., Wind, G., Amarasinghe, N., Marchant, B., Arnold, G.T., Zhang, Z., Hubanks, P.A., Holz, R.E., Yang, P., Ridgway, W.L., Riedi, J., 2017. The MODIS Cloud Optical and Microphysical Products: Collection 6 Updates and Examples from Terra and Aqua. *IEEE Transactions on Geoscience and Remote Sensing* 55, 502–525. <https://doi.org/10.1109/TGRS.2016.2610522>
- Salkind, N., 2010. Encyclopedia of Research Design. [https://doi.org/10.4135/9781412961288 NV - 0](https://doi.org/10.4135/9781412961288_NV - 0)
- Sayer, A.M., Hsu, N.C., Bettenhausen, C., Jeong, M.J., 2013. Validation and uncertainty estimates for MODIS Collection 6 "deep Blue" aerosol data. *Journal of Geophysical Research Atmospheres* 118, 7864–7872. <https://doi.org/10.1002/jgrd.50600>
- Sharif, F., Alam, K., Afsar, S., 2015. Spatio-Temporal distribution of aerosol and cloud properties over Sindh using MODIS satellite data and a HYSPLIT model. *Aerosol and Air Quality Research* 15, 657–672. <https://doi.org/10.4209/aaqr.2014.09.0200>
- Shen, H., Abduwaili, J., Ma, L., Samat, A., 2019. Remote sensing-based land surface change identification and prediction in the Aral Sea bed, Central Asia. *International Journal of Environmental Science and Technology* 16, 2031–2046. <https://doi.org/10.1007/s13762-018-1801-0>
- Shen, H., Abduwaili, J., Samat, A., Ma, L., 2016. A review on the research of modern aeolian dust in Central Asia. *Arabian Journal of Geosciences* 9. <https://doi.org/10.1007/s12517-016-2646-9>
- Stephens, G.L., Paltridge, G.W., Platt, C.M.R., 1978. Radiation Profiles in Extended Water Clouds. III: Observations. [https://doi.org/10.1175/1520-0469\(1978\)035<2133:rpiewc>2.0.co;2](https://doi.org/10.1175/1520-0469(1978)035<2133:rpiewc>2.0.co;2)
- Wood, R., 2006. Relationships between optical depth, liquid water path, droplet concentration and effective radius in an adiabatic layer cloud. University of Washington report, 2–4. https://doi.org/https://atmos.uw.edu/~robwood/papers/chilean_plume/optical_depth_relations.pdf

7 Appendix

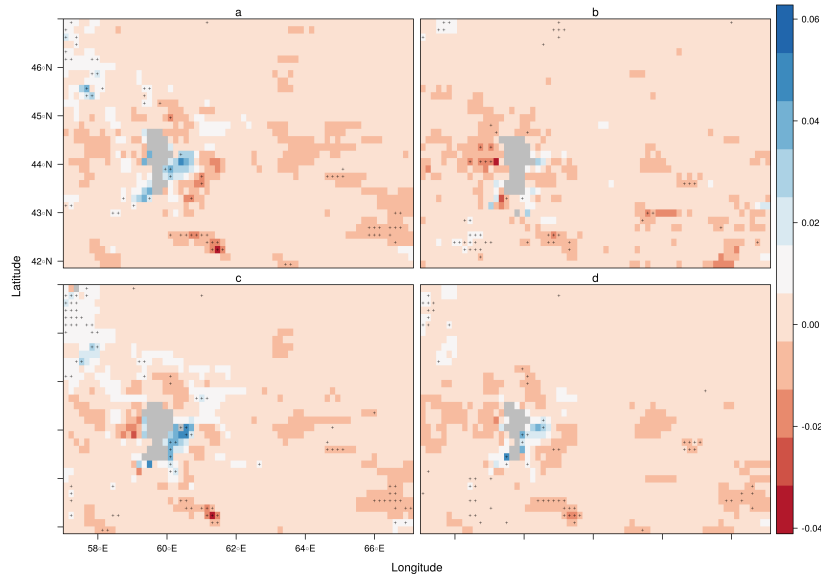


Figure 14: Spatial distribution of linear trend for AOD during spring (a), summer (b), autumn (c), and winter (d).

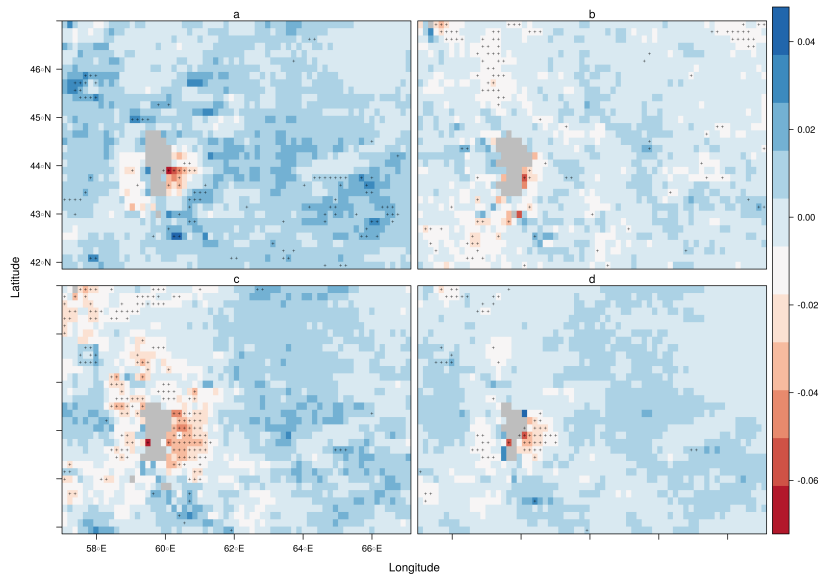


Figure 15: Spatial distribution of linear trend for AE during spring (a), summer (b), autumn (c), and winter (d).

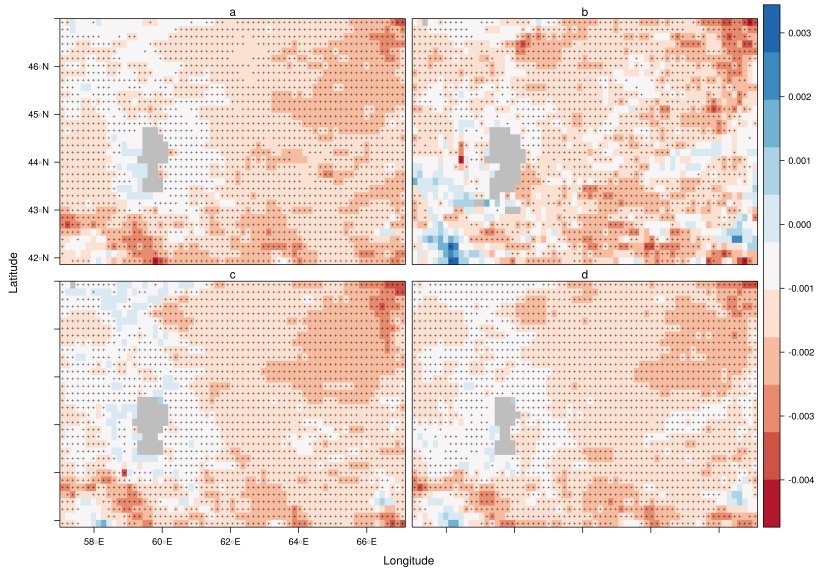


Figure 16: Spatial distribution of linear trend for SSA during spring (a), summer (b), autumn (c), and winter (d).

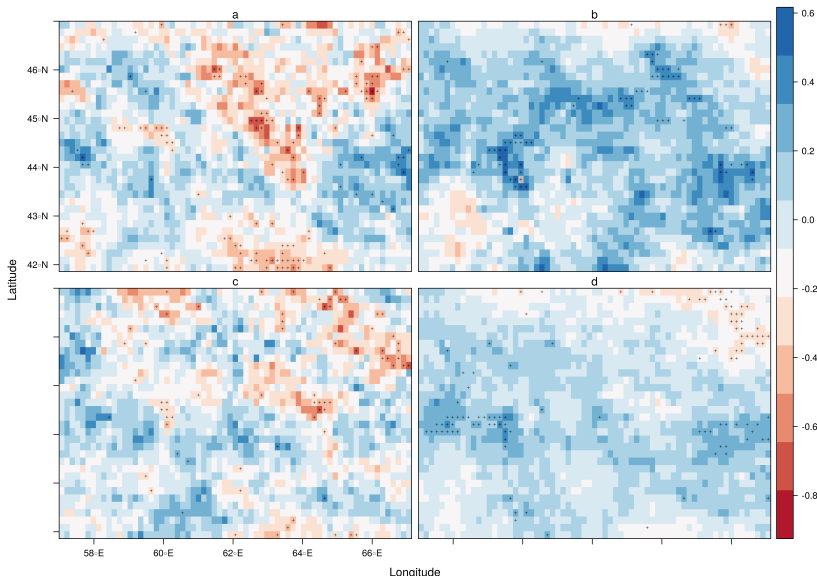


Figure 17: Spatial distribution of linear trend for COT during spring (a), summer (b), autumn (c), and winter (d).

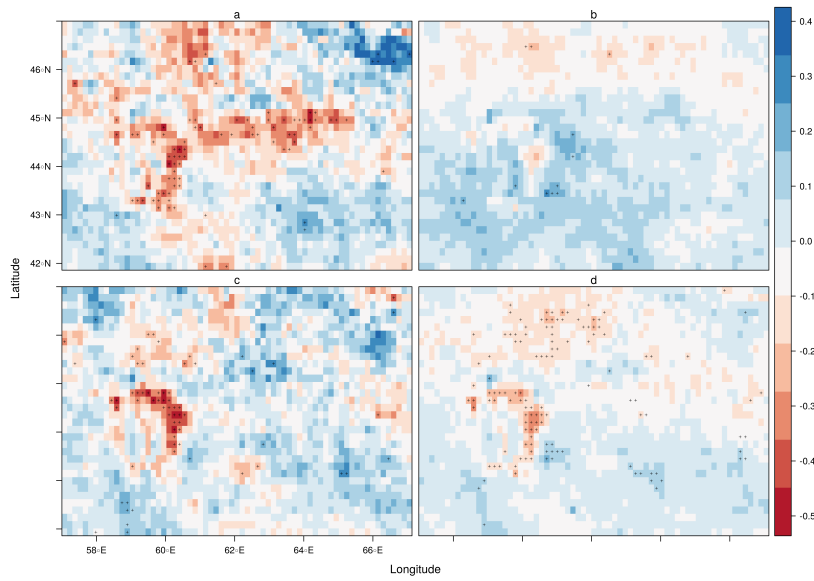


Figure 18: Spatial distribution of linear trend for CER [in microns] during spring (a), summer (b), autumn (c), and winter (d).

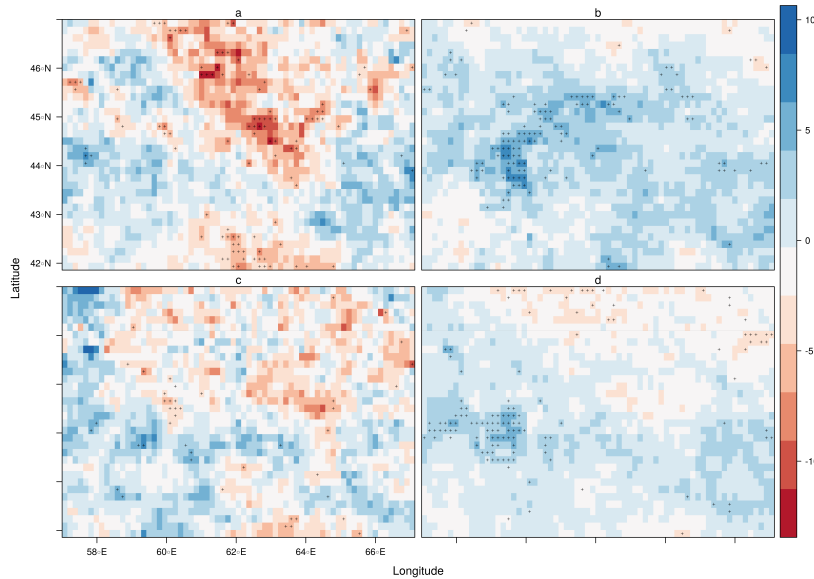


Figure 19: Spatial distribution of linear trend for CWP [in g/m²] during spring (a), summer (b), autumn (c), and winter (d).